



HAL
open science

Effect of bacterial nanocellulose on the fresh and hardened states of oil well

Juan Cruz Barría, Analía Vazquez, Jean-Michel Pereira, Diego Manzanal

► **To cite this version:**

Juan Cruz Barría, Analía Vazquez, Jean-Michel Pereira, Diego Manzanal. Effect of bacterial nanocellulose on the fresh and hardened states of oil well. *Journal of Petroleum Science and Engineering*, 2021, 199, pp.108259. 10.1016/j.petrol.2020.108259 . hal-03169623

HAL Id: hal-03169623

<https://enpc.hal.science/hal-03169623v1>

Submitted on 17 Mar 2021

HAL is a multi-disciplinary open access archive for the deposit and dissemination of scientific research documents, whether they are published or not. The documents may come from teaching and research institutions in France or abroad, or from public or private research centers.

L'archive ouverte pluridisciplinaire **HAL**, est destinée au dépôt et à la diffusion de documents scientifiques de niveau recherche, publiés ou non, émanant des établissements d'enseignement et de recherche français ou étrangers, des laboratoires publics ou privés.

Effect of bacterial nanocellulose on the fresh and hardened states of oil well cement

Juan Cruz Barría^{1,3}, Analía Vazquez², Jean-Michel Pereira³, Diego Manzanal^{1,4,5}*

⁽¹⁾ *Universidad Nacional de la Patagonia, Facultad de Ingeniería, Dpto. Ingeniería Civil, - CONICET, RP N°1 km4, Ciudad Universitaria, 9005, Comodoro Rivadavia, Argentina*

⁽²⁾ *Universidad de Buenos Aires (UBA), Facultad de Ingeniería, LAME, Av. Las Heras 2214, 1426, Buenos Aires, Argentina, Av. Las Heras 2214, Buenos Aires, Argentina*

⁽³⁾ *Navier, Ecole des Ponts, Univ Gustave Eiffel, CNRS, Marne-la-Vallée, France.*

⁽⁴⁾ *Instituto de Tecnología y Ciencias de la Ingeniería (INTECIN), Universidad de Buenos Aires (UBA), CONICET, Facultad de Ingeniería, Av. Las Heras 2214, 1426, Buenos Aires, Argentina.*

⁽⁵⁾ *ETS de Ingenieros de Caminos, Canales y Puertos, Universidad Politécnica de Madrid, c/ Prof. Aranguren 3, Ciudad Universitaria, 28040, Madrid, Spain (Current).*

*corresponding author: d.manzanal@upm.es

Abstract

The evaluation of oil well cement additives is determined by the influence on the rheological and mechanical properties of the slurry. The use of nanoadditives for cement, such as bacterial nanocellulose (BNC), has been increasing in recent years due to their high tensile strength, high Young's modulus, and thermal resistance. However, the influence of BNC addition on the mechanical properties of the cement is not widely studied. The purpose of this work is to understand the effects caused by the addition of BNC in class G cement during the fresh and hardened states. Free fluid and high-pressure consistometry tests have been carried out in the fresh state. In the hardened state, dynamic thermomechanical analyses (DMA) and uniaxial compressive strength (UCS) tests have been performed. Additionally, thermogravimetric analysis (TGA) was carried out to determine the calcium hydroxide content and the hydration degree (DOH). Results indicate that BNC modifies the slurry behavior by reducing the free fluid content and by incrementing consistency. Moreover, the calcium hydroxide content and DOH increase with the addition of BNC. The mechanical properties of BNC-cement samples are increased in terms of storage modulus and mechanical strength. These properties can improve the performance of cement used in cementing operations.

33 **Keywords**

34 Bacterial Nanocellulose – Cementing – Mechanical Performance – Thermal Analysis

35 **1. Introduction**

36 Oil well cementing is a complex procedure in wellbore operations. The cement must ensure
37 the oil well integrity and prevent links between formations (Al Ramadan et al., 2019; Kiran
38 et al., 2017). The slurry used differs from each particularly well condition, changing its
39 additives and quantities as needed. This cement mixture must meet a series of
40 requirements according to Standards, and it will be subjected to several stress loadings
41 throughout its life span. Different problems arise during these stages, but the low tensile
42 strength and cracks propagation of the set cement (Banthia and Nandakumar, 2003) and
43 its resistance to temperature are essential properties to be optimized, as well as.

44 Recently, there has been a growing interest in nanocellulose (Charreau et al., 2012).
45 Nanocellulose has a background in reducing micro-cracking (Hisseine et al., 2019, 2018).
46 Its addition to cement is very likely to induce an increment in tensile strength and prevent
47 the propagation of cracks caused by external loads. There are three types of nanocellulose
48 according to how is production; microfibrillated nanocellulose (MFC), nanocrystalline
49 cellulose (NCC), and bacterial nanocellulose (BNC).

50 Bacterial nanocellulose is an environmentally friendly material (Muhd Julkapli and Bagheri,
51 2017) produced by several bacteria types in different culture media. In particular,
52 *Gluconacetobacter xylinus* bacteria is one of the primary microbial producers of this
53 material, and its research is still ongoing (Keshk, 2014), with essential advances about
54 bacterial cultivation (Mikkelsen et al., 2009) (Vazquez et al., 2013). New studies on the
55 cost-effectiveness of culture media are making its production a significant subject of
56 interest for industrial applications (Jozala et al., 2016).

57 Recently, there has been new production of bacterial nanocellulose utilizing residues from
58 the wine industry and using steep corn liquor, which demonstrated a four-time higher yield
59 of this product in an inexpensive fermentation medium (Cerrutti et al., 2016). This increase
60 in quantity becomes significant after 21 days of incubation, and also its structure is more

1
2
3
4
5
6
7
8
9
10
11
12
13
14
15
16
17
18
19
20
21
22
23
24
25
26
27
28
29
30
31
32
33
34
35
36
37
38
39
40
41
42
43
44
45
46
47
48
49
50
51
52
53
54
55
56
57
58
59
60
61 compact and dense because it generates a more substantial number of branches that
62 intertwine with each other (Sheykhnazari et al., 2011). These denser nanocellulose fibers
63 are obtained with nanometric widths in the ranges of 18 to 57 nm and micrometers in length,
64 thus obtaining a high specific surface area material.

65 Several authors have proved that nanocellulose improves the mechanical, thermal, and
66 microstructural properties of cement-based compounds (Sun et al., 2016; Vazquez et al.,
67 2013, Barria et al., 2018, 2019, 2020a,b). Mainly, studies focused on the research of MFC,
68 and NCC. The improved properties were compressive strength, thermal performance,
69 degree of hydration, viscosity and water retention of cement (de Paula et al., 2014; Gómez
70 Hoyos et al., 2013; Mejdoub et al., 2017; Savastano et al., 2005).

71 However, there are few studies on the Bacterial nanocellulose (BNC) (Mohammadkazemi
72 et al., 2017, 2015, Barria et al. 2018, 2019). Recently, BNC has been used to modify
73 properties of the drilling fluids, enhanced oil recovery (EOR), and oil well cementing
74 (Ramasamy and Amanullah, 2020). BNC is estimated to have a similar effect of that MFC
75 and NCC on cement. The use of BNC in cement mortars shows an improvement in flexural
76 and compressive strength (Akhlaghi et al., 2020).

77 Therefore, the study of bacterial nanocellulose as an additive for oil well cement class G is
78 an exciting alternative to improve its performance in petroleum engineering applications.
79 The purpose of this work is to understand the changes due to the use of bacterial
80 nanocellulose (BNC) as an additive in class G oil-well cement during fresh and hardened
81 states. We examine the rheological behavior of an oil well cement slurry modified with
82 different percentages of BNC by performing free fluid and consistometry tests. The thermal
83 and mechanical behavior of cement class G with different BNC content is analyzed by
84 dynamic mechanical analysis (DMA) and unconfined compression strength (UCS) test. In
85 addition, the degree of hydration (DOH) of the cement paste with the addition of BNC
86 performing a thermogravimetric analysis (TGA) is investigated.

87
88

89 2. Materials

1
2 90 The cement used in this study was a Class G Portland Cement provided by PCR S.A.
3
4 91 (Petroquímica Comodoro Rivadavia S.A., Argentina). It is made with clinker and calcium
5
6 92 sulfate of high sulfate resistance grade to satisfy the chemical requirements of the
7
8 93 American Petroleum Institute (API) Specification 10A for cement (API Specification 10A,
9
10 94 2019): C₃S 52.8%, C₃A 1.6%, C₂S 21.1% and C₄AF 15.5%. The chemical composition was
11
12 95 obtained by X-ray fluorescence (XRF) and is given in Table 1. The XRF system consists of
13
14 96 an X-ray generator tube, collimators, crystals, and beam detectors. The excitation of the
15
16 97 atoms from the X-rays emits radiation that is detected by the equipment, thus quantifying
17
18 98 the chemical composition of the cement.

19
20
21 99 Bacterial nanocellulose (BNC) is a polymer derived from cellulose obtained from the
22
23 100 aerobic fermentation of bacteria of the genus *Gluconacetobacter* as the primary
24
25 101 extracellular metabolite (Charreau et al., 2012). It was provided by a spinoff of ITPN-
26
27 102 CONICET (Nanocellu-Ar) in the form of a membrane in sealed jars (Cerrutti et al., 2016).
28
29 103 The nanocellulose has a repetitive molecular structure composed of a linear backbone of
30
31 104 $\beta(1-4)$ -linked d-glucose units (Cerrutti et al., 2016; Vázquez and Pique, 2017). The
32
33 105 difference between BNC and other polymers relies on the fact that it does not possess free
34
35 106 macromolecules; it is a membrane formed by micrometric fibers of nanometric thickness.
36
37 107 Fig. 1 shows the bacteria and the interconnected nanocellulose network. These
38
39 108 membranes contain approximately 98% water and 2% BNC.

40
41
42 109 Deionized water and a superplasticizer were used in the mixture. The superplasticizer (SP)
43
44 110 additive used was the ADVA 175 LN High-Performance Water-Reducing Admixture with a
45
46 111 light-yellow liquid appearance and a density of 1.06 g/cm³. It is an additive with
47
48 112 characteristics like those of a polycarboxylate (Puertas et al., 2005).

49 113

50 114

51 115

52 116

117 **3. Sample preparations and experimental method**

118 3.1 Sample preparation

119 The slurry samples were mixed according to API specifications. A high-speed mixer with
120 an API standard blade type was used (API Specification 10A, 2019). The mixing procedure
121 consisted of 15 seconds of a rotation speed of 4.000 ± 200 rpm, and then, 35 seconds of
122 12.000 ± 500 rpm. The cement was passed through an ASTM No. 20 sieve. Each sample
123 was prepared with 792 ± 0.5 g of cement and 349 ± 0.5 g of distiller water at a temperature
124 of 23 ± 1 °C.

125 BNC membranes were wet-grinded to obtain the BNC additive. Then, the BNC-distilled
126 water mixture was conditioned in a 6.5 L Arcano ultrasonic bath with a frequency of 40.000
127 Hz for 30 minutes. This procedure breaks up the nanocellulose agglomerates fibers (Fig.
128 2). The use of the ultrasound technique improves the mechanical properties of the mixture
129 by dispersing the nanocellulose and generating a more homogeneous paste (Barbash et
130 al., 2016). The BNC proportion was determined by weighing three representative samples
131 from the additive before and after placing the samples inside an oven for 24 hours. Free
132 water was evaporated, and the average quantity of BNC obtained was approximately
133 0.46%. Afterward, the BNC-distilled water mixture was placed in the high-speed mixer
134 according to the percentage of BNC addition. Additional distiller water with SP was added
135 to obtain a W/C ratio of 0.44 by weight.

136 The addition of BNC can improve specific properties of the cement, such as an increase in
137 the degree of hydration (Cao et al., 2015), an increase in mechanical strength (Sun et al.,
138 2017), and this may reduce porosity. However, the addition also generates changes in the
139 rheological properties of the slurry (Hoyos et al., 2019). Since the previous studies
140 contemplate the changes produced by the use of different types of nanofibers, this work
141 aims to perform comprehensive research regarding the effects made only by bacterial
142 nanocellulose in the fresh and hardened states of class G cement.

143 Experiments were conducted on samples with ordinary Portland cement (PC) and cement
144 modified with percentages of BNC of 0.05, 0.10, 0.15, and 0.20 by weight of cement
145 (BWOC). Table 2 shows the details of each cement mixture.

146 3.2 Free fluid test

147 The free fluid or free water content is the volume of fluid that separates from the cement
148 slurry once the slurry remains at rest. Slurry samples of PC and modified PC with BNC
149 were performed in accordance with the API Standard 10A (API Specification 10A, 2019).
150 After the high-speed mixing (section 3.1), the slurry samples were placed in an atmospheric
151 consistometer. The atmospheric consistometer consists of a rotating cylindrical slurry
152 container equipped with a stationary pallet system. The rotational speed is 150 ± 15 RPM.
153 The vessel was kept at a controlled temperature of 27 ± 2 °C in an oil bath. After stirring
154 the slurry for 20 minutes \pm 30 seconds in the atmospheric consistometer, 760 ± 5 g of slurry
155 were transferred directly to a 0.5 L Erlenmeyer flask within 1 minute of completion of mixing.
156 The flask was kept on an anti-vibration surface for 2 hours, and the excess liquid at the top
157 was removed and measured with a pipette. The percentage of free liquid was calculated
158 using the following formula:

$$159 \quad \varphi = \frac{V_{FF} \cdot \rho}{m_s} \cdot 100 \quad (1)$$

160 Where φ is the volume fraction of free fluid expressed as a percentage, V_{FF} is the volume
161 collected with the pipette, m_s is the mass of the slurry in grams and ρ is the density of the
162 slurry in g/cm^3 which is associated with the cement density.

163 The cement density was obtained following the IRAM 1624 Standard. The cement (64 g)
164 was placed into a Le Chatelier flask containing 0.5 cm^3 of kerosene at room temperature
165 of 20 ± 2 °C and relative humidity 50%. After removing the retained air, the final reading
166 was measured after 150 ± 30 min. The cement density obtained was $3.18 \pm 0.01 \text{ g/cm}^3$.
167 The slurry density associated is 1.91 g/cm^3 .

168 3.3 High-pressure Consistometer

169 Cementing a wellbore requires a cement slurry capable of maintaining an adequate state
1 of pumpability under downhole conditions over a specific range of time. Thickening time
2 of pumpability under downhole conditions over a specific range of time. Thickening time
3 was determined with a high-temperature and high-pressure consistometer following the
4 171 API Specification 10A (API Specification 10A, 2019). The consistency of the slurry over
5 172 time is measured in Bearden units (B_C).
6 173

10 174 The cement slurry (section 3.1) was poured into a standardized container and stirred at a
11 constant speed. A ramp of temperature and pressure over time was applied to the system
12 175 until Bearden unit of consistency reached 100 B_C for a specific time. This time is known as
13 the thickening time of cement. The consistency should be less than 30B_C between 15 and
14 176 30 minutes after the beginning of the test to ensure adequate initial consistency. In the
15 field, the time to 100 Bearden units represents the amount of time cement remains
16 177 pumpable under well conditions. Bearden units are dimensionless, cannot be converted to
17 any viscosity unit, and can only be determined by the high pressure and temperature
18 178 consistometer.
19 182

30 183 3.4 Thermogravimetric analysis

32 184 Cement is a porous multi-phasic material whose main components are hydrated calcium
33 silicate, calcium hydroxide, and calcium aluminate hydrate. When comparing two different
34 185 cement types of the same age, the calculation of the hydration degree is useful. It estimates
35 the amount of anhydrous cement that has reacted with water to form the cement hydrates.
36 187 The quantity of calcium hydroxide and the hydration degree can be obtained from the
37 thermogravimetric analysis.
38 189

40 190 The determination of non-evaporable water, calcium hydroxide (CH), and hydration degree
41 (DOH) was carried out by the technique of thermogravimetric analysis. The TGA-50
42 Shimadzu equipment consists of a precision balance, where the sample was placed inside
43 192 a platinum tray in a nitrogen atmosphere and a furnace that was programmed to increase
44 the temperature from 25 to 800 °C at a constant heating rate of 10 °C/min with a constant
45 194 temperature hold at 140 °C for 15 min. Finally, the tests ended when the temperature
46 195 reached 800 °C and was maintained for 1 minute.
47 196

197 A total of five samples were crushed and analyzed in the TGA, one for each percentage of
198 nanocellulose (0%; 0.05%; 0.1%; 0.15%; 0.20% BWOC). Each sample had an approximate
199 weight of 0.008 g. The powdered material was dried at 110 °C for 24 hours to remove free
200 water (Palou et al., 2014).

201 The portlandite content is obtained with the technique proposed by (Sun et al., 2016):

$$202 \text{ CH}[\%] = \frac{74.09}{18.01} \cdot \text{WL}_{\text{CH}}[\%] \quad (2)$$

203 Where WL_{CH} is the percentage of weight loss during the test. The degree of hydration
204 (DOH) is determined by relating chemically bound water (CBW) burned to the maximum
205 CBW burned for cement. The maximum CBW value in ordinary cement is 0.23 g of bound
206 water per g of a burned sample (Pane and Hansen, 2005). Therefore, the DOH of the
207 samples studied can be calculated as the weight of CBW burned between 140 and 800 °C:

$$208 \text{ DOH}[\%] = \frac{(w_{140} - w_{800})}{0.23 \cdot w_{800}} \cdot 100 \quad (3)$$

209 3.5 Dynamic mechanical analysis

210 Cement undergoes temperature variations during its life span when it is used as annular
211 protection for the wellbore. Cement is mechanically affected when a temperature gradient
212 is applied to it.

213 In order to evaluate the thermo-mechanical properties of cement, a dynamic mechanical
214 analysis (DMA) was performed. DMA measures these properties as a function of time and
215 temperature while the material is subjected to a periodic oscillatory force (García, 2012). In
216 this case, oscillatory bending stress. The storage modulus (E') is the stiffness of the
217 material and represents the capacity of the material to store the applied energy. The loss
218 modulus (E'') is the capacity of the material to dissipate the applied energy and is also
219 related to the viscous response of the material (Jawaid et al., 2015). The vector composition
220 between the storage modulus and loss modulus is the complex modulus (shear modulus)
221 (E^*). The angle formed by these vectors is the mechanical damping factor of the material
222 (δ) (Saba and Tahir, 2016). A material that can store a large amount of applied energy will
223 have a small angle δ (high elasticity).

1
2
3
4
5
6
7
8
9
10
11
12
13
14
15
16
17
18
19
20
21
22
23
24
25
26
27
28
29
30
31
32
33
34
35
36
37
38
39
40
41
42
43
44
45
46
47
48
49
50
51
52
53
54
55
56
57
58
59
60
61
62
63
64
65

224 The dynamic mechanical analysis was performed with a Perkin-Elmer DMA 8000
225 instrument using the three-point bending mode. The deformation imposed on each pulse
226 was 0.001 mm, with a pulse frequency of 1 Hz. The test began at room temperature and
227 increased until 200 °C with a constant rate of 2 °C/min. For each pulse, the storage modulus
228 was measured. A total of 20 samples of 3 mm × 9 mm × 30 mm were tested, four for each
229 nanocellulose percentage (0%; 0.05%; 0.1%; 0.15%; 0.20% BWOC).

230 3.6 Unconfined compressive strength (UCS)

231 After mixing according to Section 3.1, the slurry was poured into standard cubic molds of 5
232 cm per side following the API specifications (ASTM International, 1999) for the subsequent
233 compressive strength tests. The molds were placed in the curing chamber at a temperature
234 of 20 ± 1 °C, and after 24 hours inside the molds, the specimens were removed and put
235 back inside the chamber. Once the curing time had passed, the axial compression test was
236 performed with planar metalheads at a velocity rate of 72 ± 7 kN/min (Fig. 3).

237 The tests were performed using bacterial nanocellulose with percentages of 0.05%, 0.1%,
238 0.15%, and 0.2%, with adequate percentages of SP to obtain workability, and were cured
239 for 7 and 28 days in order to understand the compressive strength evolution over time. The
240 results are obtained from an average of 3 samples for each percentage of BNC used. The
241 absolute variation from the average was considered for the analysis.

242 A flow chart of the testing methodology is shown in Fig. 4.

243 **Results and discussion**

244 4.1 Effect of BNC on cement slurries: free fluid content, consistency and thickening time

245 Cementing a wellbore requires a slurry capable of maintaining an adequate state of
246 flowability under downhole conditions over a specific range of time. Moreover, once the oil
247 well-cementing procedure is completed, the cement slurry requires to keep the cement
248 solids in suspension in the early and middle hydration periods. The effect of the BNC and
249 SP additions on the rheological behavior of cement slurry is analyzed through free fluid and
250 consistometer test.

1
2
3
4
5
6
7
8
9
10
11
12
13
14
15
16
17
18
19
20
21
22
23
24
25
26
27
28
29
30
31
32
33
34
35
36
37
38
39
40
41
42
43
44
45
46
47
48
49
50
51
52
53
54
55
56
57
58
59
60
61
62
63
64
65

251 Fig. 5 shows the evolution of the free fluid content [%] of Portland cement (PC) and PC +
252 0.05% BNC slurries with the addition of SP. PC slurry shows 1.89% of free fluid content
253 measured by equation 1. The free fluid of PC + 0.10% SP and PC + 0.30% SP slurries is
254 reduced by 5% and 36%, respectively. The results show a clear trend of decreasing the
255 free fluid content of the PC slurries with the increment of SP addition. However, large
256 amounts of these additions will allow more air bubbles to enter into the cement paste, thus
257 incrementing cement porosity and decreasing long-term mechanical properties and
258 durability. The reduction in the free fluid with SP has been already studied, and the
259 stabilization in the slurry occurs because of the content of polycarboxylates which
260 chemically modifies the behavior of the cement in the fresh state (Moumin and Plank,
261 2017).

262 A similar trend is observed in PC slurries with the addition of 0.05% of BNC. The free fluid
263 is significantly reduced by the addition of the BNC for a given SP value, as is shown in Fig.
264 5. For the addition of 0.10% SP, the reduction of free fluid observed in PC + 0.05%BNC
265 slurry is 76% in comparison with the PC slurry. This gap decreases as the amount of SP
266 increases. For instance, the free fluid content of PC + 0.05%BNC is reduced 52% in
267 comparison with the PC slurry for the addition of 0.35%SP. Thereby, the limitations and
268 correct doses of SP are critical.

269 Results in the modified cement slurries with BNC might be explained by the water holding
270 capacity within the mixture of the BNC (Gómez Hoyos et al., 2013). Water is adhered to
271 the surface of BNC fibers and thickens the mixture (Balea et al., 2019). We can see in
272 previous studies that no water can be extracted if the quantity of nanocellulose applied is
273 excessive (Hoyos et al., 2019).

274 Results show that when using both nanocellulose and superplasticizer, the slurry stability
275 increases, which helps to prevent a fluid breakout. This effect of fluid breakout is usually
276 accompanied by longitudinal fluid channeling, which allows gas migration (Bonett and
277 Pafitis, 1996; Nelson, 1990; Salehi et al., 2016), and by reducing this effect on the modified
278 cement, an extension of its durability can be achieved.

279 During wellbore cementing operations, if the cement slurry maintains a liquid state for a
280 short time, the constant pumping will damage the cementitious structure generated by its
281 initial setting. On the other hand, if the liquid state is maintained for a long time, it may delay
282 the commissioning of the well. With the addition of BNC to the cement slurry, an increase
283 in the yield stress is observed (Hoyos et al., 2019; Sun et al., 2016). However, there is no
284 clear understanding of the dynamic behavior of the modified slurry concerning temperature
285 changes. In order to observe the rheological behavior under temperature and pressure of
286 the cement modified with BNC, consistometry tests were performed to PC and cement with
287 the addition of 0.05% BNC. The initial consistency and the thickening time were evaluated
288 for different percentages of SP to obtain slurry workability similar to PC. The results are
289 shown in Table 3.

290 Three different tests are shown in Fig. 6; tests 1 (Portland cement), 5 and test 6 (Cement
291 + 0.05% BNC). Consistencies are shown along the Y-axis versus time along the X-axis.
292 Test 1 describes the normal curve for unmodified class G oil-well cement. In the cases of
293 BNC-modified slurries with additions of SP less than 0.3%, samples quickly become very
294 viscous, reducing workability with consistency values above the tolerable value (30 Bc).
295 This behavior is different from other polymers, where it has been found that a natural
296 cellulose polymer increases thickening time (Abbas et al., 2013). The difference with their
297 experiment is that hydroxypropylmethylcellulose acted as a retarding agent to cement
298 setting, allowing the slurry to remain in a liquid state. In our case, BNC acts like a water
299 retainer, removing water used for workability and adsorbing it. This effect reduces the initial
300 cement hydration, but at the same time, it considerably increases consistency in Bearden
301 units, reducing thickening time. BNC has a width range between 18 to 57 nm and
302 micrometers in length (Cerrutti et al., 2016), which can lead to a specific surface area
303 variance between 150 and 250 m²/g (Li et al., 2017). Hence, the water employed in cement
304 workability is now reduced to wet this new surface. The addition of 0.1% of BNC
305 considerably increases the yield stress (Hoyos et al., 2019), while an increment of 0.4%
306 leads to a cement paste that is impossible to flow.

1
2
3
4
5
6
7
8
9
10
11
12
13
14
15
16
17
18
19
20
21
22
23
24
25
26
27
28
29
30
31
32
33
34
35
36
37
38
39
40
41
42
43
44
45
46
47
48
49
50
51
52
53
54
55
56
57
58
59
60
61
62
63
64
65

307 The consistency of BNC-modified slurries with additions of SP of 0.35% approximates to
308 the PC behavior. Despite this behavior being erratic through time, the final thickening time
309 is similar to the reference cement. However, BNC-modified slurries with additions of SP of
310 0.35% have an initial consistency higher than the PC slurry, due to the higher initial yield
311 stress. On the other hand, the modified samples with additions of SP of 0.4% present a
312 smaller initial consistency, and the thickening time is 25 min longer than the PC and
313 modified samples with additions of SP of 0.35%. This effect is caused by the SP, which
314 makes the mixture more fluid and needs more time to thicken. Larger quantities of SP
315 reduce the probability of the hydration reaction and the precipitation of solid cement
316 particles during the first hours, allowing the sample to remain in a liquid state for longer.

317 4.2 Effect of BNC on the degree of hydration

318 TGA and DrTGA results are shown in Fig. 7 and Fig. 8, respectively. The content of each
319 material phase was calculated by drawing three tangential lines on the TGA graph, and the
320 vertical difference of mass percentage between the intersections is considered the
321 decomposition of the material (Marsh and Day, 1988; Sun et al., 2016; Wild and Khatib,
322 1997). The continuous loss of mass on the graph is due to the dehydration of CSH and
323 other compounds that starts at 105 °C and continue until the end of the test (DeJong and
324 Ulm, 2007; Palou et al., 2014). The drop in mass between 420 and 480 °C is due to the
325 portlandite decomposition into Ca^{2+} ions and 2HO^- from which CaO and $\text{H}_2\text{O}\uparrow$ are produced
326 (De Weerd et al., 2011). We also can see a small drop between 600 and 650 °C, which is
327 the decomposition of calcite. But considering that this cement was kept under alkaline
328 distilled water with negligible carbonation in the samples during 28 days (Tuutti, 1982) and
329 given the fact that the samples were dried in an oven at 110 °C during 24 hours, we can
330 assume that this calcite is, in fact, portlandite that was carbonated during drying and formed
331 into calcite due to accelerated carbonation in the oven, increasing the CO_2 uptake (Liu et
332 al., 2001). The shape of the curves is similar for those samples with and without additions,
333 and they do not show new products due to BNC or SP addition (Ma et al., 2011). The curves
334 of 0.05% and 0.15% content of BNC cannot be distinguished.

1
2
3
4
5
6
7
8
9
10
11
12
13
14
15
16
17
18
19
20
21
22
23
24
25
26
27
28
29
30
31
32
33
34
35
36
37
38
39
40
41
42
43
44
45
46
47
48
49
50
51
52
53
54
55
56
57
58
59
60
61
62
63
64
65

335 Portlandite content increases with the BNC content, as we can see in Table 4. The BNC
336 water retainer effect generates an additional source of water, which is enhancing the
337 generation of hydration products (Gómez Hoyos et al., 2013; Hisseine et al., 2019). On the
338 other hand, the degree of hydration (DOH) is higher in all percentages of BNC compared
339 to PC. Similar behavior can be found in the literature (Sun et al., 2016). The DOH values
340 are underestimated because they were obtained at 800°C instead of 1100°C. However, it
341 shows a trend in all the samples analysed.

342 Cement hydration and development of the microstructure over time are complex processes
343 whose study is not the objective of this work. However, an explanation of the increment in
344 DOH and CH content is necessary. The surface free energy (SFE) is an indicator that can
345 characterize if a surface is more or less hydrophobic. The sum of the dispersive and polar
346 components gives the SFE. According to the literature, dispersive surface energy can
347 increase up to 138% by adding BNC to the cement sample (Mohammadkazemi et al.,
348 2017). This causes more hydration reactions due to the increased amount of water on the
349 surfaces of the cement microstructure. Therefore, the increase in SFE explains the
350 increase in portlandite (CH) and DOH. Calorimetry tests on nanocellulose materials have
351 shown an increase in heat release (Cao et al., 2015; Lee et al., 2019), thus obtaining a
352 higher hydration degree. However, initially, it acts as a retarder for cement (Cao et al.,
353 2016; Fu et al., 2017). Hisseine (Hisseine et al., 2019) suggested that the heat increment
354 during the calorimetry test is associated with the alkaline hydrolysis of cellulose, which
355 promotes cement hydration. Furthermore, cellulose filaments tend to release water during
356 hydration (Hisseine et al., 2018). In our experiments, BNC is in line with the nanocellulose
357 effects on cement mentioned in the literature, incrementing the hydration degree and
358 portlandite content.

359 4.3 Effect of BNC on the mechanical performance: dynamic mechanical analysis and 360 unconfined compressive strength

1
2 362 The stiffness of the material is calculated from the deformation under load. The storage
3 modulus E' is a function of the elastic properties of the samples, and it is analogous to the
4 363 static modulus of elasticity or Young's Modulus.
5

6 364 The values obtained by the DMA results of the storage modulus are observed on a
7 logarithmic scale in Fig. 9. This modulus is reduced by increasing temperature. Samples
8 365 with 0.15% and 0.20% of BNC maintain higher magnitudes than PC from 20°C to 200°C,
9 while 0.05% of BNC has lower values throughout the test. BNC can maintain properties
10 366 while the temperature is rising in the medium, which is traceable to its thermal stability up
11 to 350 °C (Hoyos et al., 2019). The reduction of the stiffness (E' values) during the first step
12 until 110 °C is due to dehydration of the free adsorbed water and some interlayered water
13 367 (Sereda et al., 1966) which speed up the start to micro-cracking of the sample (Evans and
14 Marathe, 1968).
15 372

16 373 In Fig. 10, we normalized the storage moduli to their initial values. The normalized storage
17 modulus is obtained by dividing the module measured at a certain temperature (T_i) over its
18 374 initial value (T_0) for each tested sample. An important drop is observed between 110 and
19 375 140 °C, where cement samples lose between 80% and 50% of their storage modulus. This
20 drop can be explained due to water evaporation from the samples and to CSH dehydration,
21 376 starting at approximately 110 °C (Foray-thevenin et al., 2006). The dehydration begins to
22 degrade the properties of the cementitious matrix because the water acts as a stabilizer of
23 the CSH structure. Here, cement with 0.15% of BNC has a better performance than PC
24 381 and cement modified with 0.05% or 0.20% of BNC. These samples are the most stable
25 mixtures, due to that quantity is better distributed in the sample. BNC acts like water
26 382 molecules and pulls apart the CSH interlayer. For the other samples, a more rapid collapse
27 of the CSH structure with dehydration occurs. More sliding sites, increment in the internal
28 383 friction, and a faster reduction of the elasticity consequently decreases quicker the value
29 of E with temperature (Alizadeh et al., 2011). At 130°C, PC shows a lost 70% of its modulus,
30 384 while samples with 0.15% of BNC only lost 30%.
31
32
33
34
35
36
37
38
39
40
41
42
43
44
45
46
47
48
49
50
51
52
53
54
55
56
57
58
59
60
61
62
63
64
65

388 On the other hand, the storage modulus of the 0.05% BNC sample is smaller than the PC
389 samples for most of the test, except between 130 and 160 °C. However, the normalized
390 module graph shows better behavior after 120°C. This means that this small addition of
391 BNC changes the thermal properties but does not change the bending strength.

392 In Fig. 11, temperature provokes a significant impact on the PC sample, inducing higher
393 $\tan \delta$, which represents the material resistance to be deformed by temperature. This effect
394 starts to be detected at 150 °C and until 200 °C. On the other hand, cement with a higher
395 percentage of BNC (0.15% and 0.20%) has not been affected as the previous one. It has
396 maintained a lower loss modulus factor (85% less than PC at 200 °C), except for the
397 percentage of 0.05%, where the reduction is 50%. Considering the analysis of
398 nanostructure performed by Alizadeh et al. (Alizadeh et al., 2011), the behavior of $\tan \delta$ of
399 PC and 0.05% of BNC is different from 0.15 and 0.20 % BNC. This can be related to the
400 different microstructure generated due to the formation of aggregates of BNC in the mixture
401 with PC. Alizadeh et al. related the higher $\tan \delta$ value to higher E'' , and sliding frictional
402 effects that occur when water is evaporated from adsorbed water because water restrains
403 the CSH sheets. The decrease of $\tan \delta$ or damping effect is the consequence of higher
404 rigidity of the nanostructure. This is the result of a higher bridging of the CSH sheets due
405 to the increases in the number of strong bonds between Si and O or Si-O_Ca. These bonds
406 are due to the dehydration of water interlayer of CSH, which is higher for a higher content
407 of BNC.

408 As seen before on the microstructure of cement, PC has the lowest hydration degree of the
409 samples. The lower quantities and shorter length chains of CH are making this cement
410 more susceptible to creep (Pourbeik et al., 2013), while samples with higher hydration
411 degrees are withstanding the oscillatory loading. On the other hand, cement samples under
412 bending mode are very dependent on the material tensile strength. Fatigue crack
413 propagation depends on the applied stress, the initial crack size, and the material
414 toughness to fracture. As the applied stresses are the same (bending load and temperature
415 rate changes), the samples reinforced with BNC induce two types of changes. The first

416 change occurs on the pre-testing cracking size (tensile strength improvement) and the
417 second one on the fracture toughness (hydration improvement). These changes explain
418 the behavior of the samples at 200°C, where all modified samples with BNC have shown
419 higher storage modulus than PC, except with 0.05%.

420 Previous studies have worked with other polymers and also found that fibers add more
421 flexural strength in cement (Jamshidi and Karimi, 2009; Parveen et al., 2017). Our results
422 show this trend on flexural strength, and now it shows improvement under thermal stresses.
423 Samples of 0.15 and 0.20% BNC increase the properties at room temperature and up to
424 200°C

425 The tensile strength of cement samples is around 10% of the unconfined compressive
426 strength for Portland cement. The addition of BNC increases the tensile stress reinforcing
427 the samples and increasing compressive strength (Parveen et al., 2017).

428 The compressive strength of BNC-cement mixtures was determined for samples cured in
429 a water bath at 20 °C during 7 and 28 days.

430 Fig. 12 shows the normalized compressive strength of cement as a function of BNC
431 percentages cured for 7 and 28 days. The strength values (Δ) are normalized to the
432 strength value obtained after 7 days of curing in PC cement (Δ_0). The error bars show the
433 absolute variation obtained in the tests. The unconfined compressive strength of PC, and
434 the mixtures PC + 0.05%, 0.10%, 0.15% and 0.20% BNC for different curing times is
435 presented in Fig. 13. The errors in the PC and 0.05% samples are very small in Fig 12, so
436 their error bar is not visible in the graph. To plot Figure 13, only the average values of the
437 results were used.

438 The results show an enhancement in strength for cement samples with the addition of BNC.
439 However, PC + 0.15% BNC and PC + 0.20% BNC samples at 7 days shown a decrease in
440 the strength influenced by the segregation in the mixture due to the SP (Xiaofeng et al.,
441 1990). It is known that other types of nanocellulose increases compressive strength as well
442 (Hisseine et al., 2019; Lee et al., 2019; Mejdoub et al., 2017). The increase in tensile stress
443 (Cao et al., 2015), compressive strength, and hydration degree support the use of BNC as

1
2
3
4
5
6
7
8
9
10
11
12
13
14
15
16
17
18
19
20
21
22
23
24
25
26
27
28
29
30
31
32
33
34
35
36
37
38
39
40
41
42
43
44
45
46
47
48
49
50
51
52
53
54
55
56
57
58
59
60
61
62
63
64
65

444 a long-term reinforcement. The hydrophilic characteristic of BNC to avoid faster water loss
445 during cement hydration is preventing the propagation of thermally induced cracking (Balea
446 et al., 2019). By decreasing these cracks, the probability of failure through them for the
447 same stress is decreased (Banthia and Nandakumar, 2003; Lee et al., 2019), allowing the
448 bulk sample to withstand more loading.

449 The strength tends to increase with the percentage of nanocellulose. A small increment in
450 BNC (0.05%) produces an important increment in compressive strength, both at 7 days
451 and at 28 days. The addition of 0.05% BNC increases by 18% and 20% the strength in
452 comparison with cement sample (PC) cured at 7 days and 28 days, respectively. Other
453 authors also obtained a significant rise in strength for small percentages of nanocellulose
454 addition (Hisseine et al., 2019; Sun et al., 2016). The results are encouraging the use of
455 BNC in future admixtures due to its low amount of incorporation and low change in the
456 viscosity.

457 **5. Conclusions**

458 An experimental study regarding the effects produced by the addition of bacterial
459 nanocellulose (BNC) between 0.05% to 0.20% BWOC to cement was carried out. Free
460 fluid tests, high-pressure consistometry tests, thermogravimetric analysis,
461 thermomechanical analysis, and uniaxial compressive strength tests were performed.

462 Results indicate that the addition of BNC between 0.05% to 0.20% BWOC produces an
463 important decrease in the amount of free fluid.

464 The addition of BNC reduces the thickening time of cement slurry, and a dispersive agent
465 is needed to maintain the fluidity of the mixture. Nevertheless, more significant amounts of
466 dispersant increase the thickening time for the same amount of nanocellulose.

467 The thermogravimetric analysis shows an increment in hydration products and hydration
468 degree as the percentage of bacterial nanocellulose increases due to its hydrophilic
469 properties.

1
2 471 The dynamic mechanical analysis shows an improvement in the thermoelastic behavior of
3
4 472 cement pastes by using large percentages of BNC, mainly by its thermal stability and its
5
6 473 tensile reinforcement.

7
8 474 The use of BNC in cement has shown an increment in strength development at 7 and 28
9
10 475 days. All the mixtures using bacterial nanocellulose have increased the compressive
11
12 476 strength development over time.

13 477 In summary, the 0.05% additions BWOC of bacterial nanocellulose have shown good
14
15 478 performance for tests with fresh and hardened cement samples. In fresh cement samples,
16
17 479 the workability is achieved with small amounts of superplasticizer, and the free fluid is
18
19 480 suitable to be used in the consistometer. The mechanical properties obtained during
20
21 481 thermo-mechanical tests (DMA) are similar to ordinary cement, but a significant increment
22
23 482 in compressive strength is observed. The results are beneficial up to 0.20% BWOC of BNC
24
25 483 used, although a more considerable amount of superplasticizer is needed to maintain the
26
27 484 fresh samples' fluidity.

28
29 485 The addition of bacterial nanocellulose between 0.05% to 0.20% BWOC improves the
30
31 486 mechanical properties of the cement due to its tensile strength and crack inhibition. Another
32
33 487 reason for this might be the increase in hydration degree, which generates more CSH and
34
35 488 CH that increase its strength. The water retention of BNC increases its initial consistency.
36
37 489 However, it produces a considerable decrease in its free fluid content, which enhances its
38
39 490 hydration. Further analysis of microstructure is underway to characterize the modified
40
41 491 cement.

42
43 492 Bacterial nanocellulose proves to be an inexpensive, renewable, and high-strength material
44
45 493 that can be used as an additive to oil well cement. These characteristics can benefit the
46
47 494 cement used during well-cementing operations. Due to its low free fluid content, the
48
49 495 probability of fluid migration in the well may be reduced. The increase in thermal and
50
51 496 mechanical strength can improve the performance of the cement sheath surrounding the
52
53 497 casing, having a better behavior when supporting the stresses generated by temperature
54
55
56
57
58
59
60
61
62
63
64
65

499 **Acknowledgment**

500 The first author gratefully acknowledges the fellowship granted by CONICET (National
 501 Scientific and Technical Research Council – Argentina). The authors also acknowledged
 502 the financial support of “*Universidad Nacional de la Patagonia San Juan Bosco*” (Project
 503 UNPSJB PI1614 – 80020190200006IP, Resol R/9N°207-2020 CRD1365 FI004/17) and
 504 the Agency of Scientific and Technological Promotion (Agencia Nacional de Promoción
 505 Científica y Tecnológica) from Ministry of Science and Technology of Argentine Republic.
 506 (Projects PICT 2016-4543). The authors express their gratitude to Petroquímica Comodoro
 507 Rivadavia S.A. and its technical staff for helping with the performed tests.

508 **Abbreviations**

509	<i>API:</i>	<i>American Petroleum Institute</i>
510	<i>BNC:</i>	<i>Bacterial nanocellulose</i>
511	<i>BWOC:</i>	<i>By weight of cement</i>
512	<i>C₃S:</i>	<i>Alite</i>
513	<i>C₃A:</i>	<i>Calcium aluminate</i>
514	<i>C₂S:</i>	<i>Belite</i>
515	<i>C₄AF:</i>	<i>Calcium alumino-ferrite</i>
516	<i>CH:</i>	<i>Calcium hydroxide</i>
517	<i>CSH:</i>	<i>Calcium silicate hydrate</i>
518	<i>CBW:</i>	<i>Chemical bound water</i>
519	<i>DMA:</i>	<i>Dynamic mechanical analysis</i>
520	<i>DOH:</i>	<i>Degree of hidration</i>
521	<i>DrTGA:</i>	<i>Derivative hermogravimetric analysis</i>
522	<i>EOR:</i>	<i>Enhanced oil recovery</i>
523	<i>MFC:</i>	<i>Microfibrillated nanocellulose</i>
524	<i>NCC:</i>	<i>Nanocrystalline cellulose</i>
525	<i>PC:</i>	<i>Portland Cement</i>
526	<i>SP:</i>	<i>Superplasticizer</i>
527	<i>TGA:</i>	<i>Thermogravimetric analysis</i>
528	<i>UCS:</i>	<i>Uniaxial compressive strength</i>
529	<i>W/C:</i>	<i>Water to cement ratio</i>
530	<i>XRF:</i>	<i>X-ray fluorescence</i>

531 **Nomenclature**

- 1
2 532 δ : *Mechanical damping factor []*
3
4 533 Δ_0 : *PC compressive strength at 7 days [MPa]*
5
6 534 Δ : *Sample compressive strength [MPa]*
7
8 535 ρ : *Slurry density [g/ cm³]*
9
10 536 φ : *volume fraction of free fluid [%]*
11
12 537 m_s : *Slurry mass [g]*
13
14 538 E : *Young's Modulus [MPa]*
15
16 539 E' : *Material stiffness [MPa]*
17
18 540 E'' : *Loss modulus [MPa]*
19
20 541 E^* : *Complex modulus [MPa]*
21
22 542 T_0 : *Initial chamber temperature [°C]*
23
24 543 T_i : *Chamber temperature at time i [°C]*
25
26 544 V_{FF} : *Collected volume [cm³]*
27
28 545 WL_{CH} : *CH weight loss [%]*
29
30 546 W_{140} : *Weight burned at 140° [g]*

547
548 **References**

- 549 Abbas, G., Irawan, S., Kumar, S., Elrayah, A.A.I., 2013. Improving Oil well Cement Slurry
550 Performance Using Hydroxypropylmethylcellulose Polymer. *Adv. Mater. Res.* 787,
551 222–227. <https://doi.org/10.4028/www.scientific.net/amr.787.222>
552 Akhlaghi, M.A., Bagherpour, R., Kalhori, H., 2020. Application of bacterial nanocellulose
553 fibers as reinforcement in cement composites. *Constr. Build. Mater.* 241, 118061.
554 <https://doi.org/10.1016/j.conbuildmat.2020.118061>
555 Al Ramadan, M., Salehi, S., Kwatia, G., Ezeakacha, C., Teodoriu, C., 2019. Experimental
556 investigation of well integrity: Annular gas migration in cement column. *J. Pet. Sci.*
557 *Eng.* 179, 126–135. <https://doi.org/10.1016/j.petrol.2019.04.023>
558 Alizadeh, R., Beaudoin, J.J., Raki, L., 2011. Mechanical properties of calcium silicate
559 hydrates. *Mater. Struct. Constr.* 44, 13–28. [https://doi.org/10.1617/s11527-010-](https://doi.org/10.1617/s11527-010-9605-9)
560 9605-9
561 API Specification 10A, 2019. Specification for Cements and Materials for Well Cementing,

- 562 Twenty-Fif. ed, American Petroleum Institute. Northwest Washington, DC.
- 1
2 563 ASTM International, 1999. ASTM C109: Standard Test Method for Compressive Strength
3
4 564 of Hydraulic Cement Mortars. Am. Soc. Test. Mater. 04, 1–6.
5
6 565 <https://doi.org/10.1520/C0109>
7
- 8
9 566 Balea, A., Fuente, E., Blanco, A., Negro, C., 2019. Nanocelluloses: Natural-based
10
11 567 materials for fiber- reinforced cement composites. A critical review. Polymers
12
13 568 (Basel). 11. <https://doi.org/10.3390/polym11030518>
14
- 15 569 Banthia, N., Nandakumar, N., 2003. Crack growth resistance of hybrid fiber reinforced
16
17 570 cement composites. Cem. Concr. Compos. 25, 3–9. <https://doi.org/10.1016/S0958->
18
19 571 [9465\(01\)00043-9](https://doi.org/10.1016/S0958-9465(01)00043-9)
20
21
- 22 572 Barbash, V.A., Yaschenko, O. V., Alushkin, S. V., Kondratyuk, A.S., Posudievsky, O.Y.,
23
24 573 Koshechko, V.G., 2016. The Effect of Mechanochemical Treatment of the Cellulose
25
26 574 on Characteristics of Nanocellulose Films. Nanoscale Res. Lett. 11, 16–23.
27
28 575 <https://doi.org/10.1186/s11671-016-1632-1>
29
30
- 31 576 Barria, J.C., Martin, C., Pique, T., Pereira, J.M., Manzanal, D., 2018. Analysis of modified
32
33 577 cement paste in the context of CO2 geological storage. International Symposium of
34
35 578 Energy Geotechnics. Lugar: Laussane, Pages 402-409. Publisher: Springer, Cham.
36
37 579 Online ISBN 978-3-319-99670-7. <https://doi.org/10.1007/978-3-319-99670-7>.
38
39
- 40 580 Barria, J.C., Manzanal, Pereira, J.M., 2019. CO2 geological storage: Performance of
41
42 581 Cement-Rock interface. XVI Pan-American Conference on Soil Mechanics and
43
44 582 Geotechnical Engineering 17-20 November 2019. Cancun, México. DOI:
45
46 583 [10.3233/STAL190359](https://doi.org/10.3233/STAL190359)
47
48
- 49 584 Barria, J.C., Manzanal, Pereira, J.M., Ghabezloo, S., 2020a. CO2 Geological storage:
50
51 585 Microstructure and mechanical behaviour of cement modified with biopolymers after
52
53 586 carbonation. E3S Web Conf. Vol. 205, 2020. 2nd International Conference on
54
55 587 Energy Geotechnics (ICEGT 2020), section: CO2 Sequestration and Deep
56
57 588 Geothermal Energy 18 November 2020: DOI: [10.1051/e3sconf/202020502007](https://doi.org/10.1051/e3sconf/202020502007)
58
59
- 60 589 Barria, J.C., Pereira, J.M., Manzanal, D., 2020b. Cement with bacterial nanocellulose
61
62
63
64
65

590 cured at high temperature: mechanical performance in the context of CO₂ geological
1 storage. *Geomechanics for Energy and the Environment*. Under review.
2
3
4 592 Bonett, A., Pafitis, D., 1996. Getting to the root of gas migration. *Oilf. Rev.* 8, 36–49.
5
6 593 Cao, Y., Tian, N., Bahr, D., Zavattieri, P.D., Youngblood, J., Moon, R.J., Weiss, J., 2016.
7
8 594 The influence of cellulose nanocrystals on the microstructure of cement paste. *Cem.*
9
10 595 *Concr. Compos.* 74, 164–173. <https://doi.org/10.1016/j.cemconcomp.2016.09.008>
11
12 596 Cao, Y., Zavaterri, P., Youngblood, J., Moon, R., Weiss, J., 2015. The influence of
13
14 597 cellulose nanocrystal additions on the performance of cement paste. *Cem. Concr.*
15
16 598 *Compos.* 56, 73–83. <https://doi.org/10.1016/j.cemconcomp.2014.11.008>
17
18 599 Cerrutti, P., Roldán, P., García, R.M., Galvagno, M.A., Vázquez, A., Foresti, M.L., 2016.
19
20 600 Production of bacterial nanocellulose from wine industry residues: Importance of
21
22 601 fermentation time on pellicle characteristics. *J. Appl. Polym. Sci.* 133.
23
24 602 <https://doi.org/10.1002/app.43109>
25
26 603 Charreau, H., L. Foresti, M., Vazquez, A., 2012. Nanocellulose Patents Trends: A
27
28 604 Comprehensive Review on Patents on Cellulose Nanocrystals, Microfibrillated and
29
30 605 Bacterial Cellulose. *Recent Pat. Nanotechnol.* 7, 56–80.
31
32 606 <https://doi.org/10.2174/18722105130106>
33
34 607 de Paula, J.N., Calixto, J.M., Ladeira, L.O., Ludvig, P., Souza, T.C.C., Rocha, J.M., de
35
36 608 Melo, A.A.V., 2014. Mechanical and rheological behavior of oil-well cement slurries
37
38 609 produced with clinker containing carbon nanotubes. *J. Pet. Sci. Eng.* 122, 274–279.
39
40 610 <https://doi.org/10.1016/j.petrol.2014.07.020>
41
42 611 De Weerd, K., Haha, M. Ben, Le Saout, G., Kjellsen, K.O., Justnes, H., Lothenbach, B.,
43
44 612 2011. Hydration mechanisms of ternary Portland cements containing limestone
45
46 613 powder and fly ash. *Cem. Concr. Res.* 41, 279–291.
47
48 614 <https://doi.org/10.1016/j.cemconres.2010.11.014>
49
50 615 DeJong, M.J., Ulm, F.J., 2007. The nanogranular behavior of C-S-H at elevated
51
52 616 temperatures (up to 700 °C). *Cem. Concr. Res.* 37, 1–12.
53
54 617 <https://doi.org/10.1016/j.cemconres.2006.09.006>
55
56
57
58
59
60
61
62
63
64
65

- 618 Evans, R.H., Marathe, M.S., 1968. Microcracking and stress-strain curves for concrete in
1 tension. *Matériaux Constr.* 1, 61–64. <https://doi.org/10.1007/BF02479001>
2
3
4 620 Foray-thevenin, G., Vigier, G., Vassoille, R., Orange, G., 2006. Characterization of
5
6 621 cement paste by dynamic mechanical Part I : operative conditions 56, 129–137.
7
8 622 <https://doi.org/10.1016/j.matchar.2005.10.007>
9
10 623 Fu, T., Montes, F., Suraneni, P., Youngblood, J., Weiss, J., 2017. The influence of
11
12 624 cellulose nanocrystals on the hydration and flexural strength of Portland cement
13
14 625 pastes. *Polymers (Basel)*. 9. <https://doi.org/10.3390/polym9090424>
15
16 626 García, C., 2012. Caracterización térmica y mecánica de polibutilentereftalato (PBT).
17
18 627 Univ. politécnica Cart. Universidad Politécnica de Cartagena.
19
20 628 Gómez Hoyos, C., Cristia, E., Vázquez, A., 2013. Effect of cellulose microcrystalline
21
22 629 particles on properties of cement based composites. *Mater. Des.* 51, 810–818.
23
24 630 <https://doi.org/10.1016/j.matdes.2013.04.060>
25
26 631 Hisseine, O.A., Omran, A.F., Tagnit-Hamou, A., 2018. Influence of cellulose filaments on
27
28 632 cement paste and concrete. *J. Mater. Civ. Eng.* 30, 1–14.
29
30 633 [https://doi.org/10.1061/\(ASCE\)MT.1943-5533.0002287](https://doi.org/10.1061/(ASCE)MT.1943-5533.0002287)
31
32 634 Hisseine, O.A., Wilson, W., Sorelli, L., Tolnai, B., Tagnit-Hamou, A., 2019. Nanocellulose
33
34 635 for improved concrete performance: A macro-to-micro investigation for disclosing the
35
36 636 effects of cellulose filaments on strength of cement systems. *Constr. Build. Mater.*
37
38 637 206, 84–96. <https://doi.org/10.1016/j.conbuildmat.2019.02.042>
39
40 638 Hoyos, C.G., Zuluaga, R., Gañán, P., Pique, T.M., Vazquez, A., 2019. Cellulose
41
42 639 nanofibrils extracted from fique fibers as bio-based cement additive. *J. Clean. Prod.*
43
44 640 235, 1540–1548. <https://doi.org/10.1016/j.jclepro.2019.06.292>
45
46 641 Jamshidi, M., Karimi, M., 2009. Characterization of Polymeric Fibers as Reinforcements
47
48 642 of Cement-Based Composites. *J. Appl. Polym. Sci.* 115, 2779–2785.
49
50 643 <https://doi.org/10.1002/app>
51
52 644 Jawaid, M., Khalil, H.P.S.A., Hassan, A., Dungani, R., Hadiyane, A., 2015. Composites :
53
54 645 Part B Effect of jute fibre loading on tensile and dynamic mechanical properties of oil
55
56
57
58
59
60
61
62
63
64
65

646 palm epoxy composites. *Compos. Part B* 45, 619–624.
1
2 647 <https://doi.org/10.1016/j.compositesb.2012.04.068>
3
4 648 Jozala, A.F., Lencastre-novaes, L.C. De, Lopes, A.M., Santos-ebinuma, V.D.C., Mazzola,
5
6 649 P.G., Pessoa-jr, A., 2016. Bacterial nanocellulose production and application : a 10-
7
8 650 year overview. *Appl. Microbiol. Biotechnol.* 100, 2063–2072.
9
10 651 <https://doi.org/10.1007/s00253-015-7243-4>
11
12 652 Keshk, S.M.A.S., 2014. Bacterial Cellulose Production and its Industrial Applications. *J.*
13
14 653 *Bioprocess. Biotech.* 4. <https://doi.org/10.4172/2155-9821.1000150>
15
16 654 Kiran, R., Teodoriu, C., Dadmohammadi, Y., Nygaard, R., Wood, D., Mokhtari, M., Salehi,
17
18 655 S., 2017. Identification and evaluation of well integrity and causes of failure of well
19
20 656 integrity barriers (A review). *J. Nat. Gas Sci. Eng.* 45, 511–526.
21
22 657 <https://doi.org/10.1016/j.jngse.2017.05.009>
23
24 658 Klemm, D., Schumann, D., Kramer, F., Heßler, N., Hornung, M., Marsch, S.,
25
26 659 *Gesichtschirurgie, K.-, Chirurgie, P., Jena, F., Allee, E., V, P.J.*, 2006.
27
28 660 Nanocelluloses as Innovative Polymers in Research and Application. *Adv. Polym.*
29
30 661 *Sci.* 49–96. https://doi.org/10.1007/12_097
31
32 662 Lee, H.J., Kim, S.K., Lee, H.S., Kim, W., 2019. A Study on the Drying Shrinkage and
33
34 663 Mechanical Properties of Fiber Reinforced Cement Composites Using Cellulose
35
36 664 Nanocrystals. *Int. J. Concr. Struct. Mater.* 13. [https://doi.org/10.1186/s40069-019-](https://doi.org/10.1186/s40069-019-0351-2)
37
38 665 [0351-2](https://doi.org/10.1186/s40069-019-0351-2)
39
40 666 Li, Z., Ahadi, K., Jiang, K., Ahvazi, B., Li, P., Anyia, A.O., Cadien, K., Thundat, T., 2017.
41
42 667 Freestanding hierarchical porous carbon film derived from hybrid nanocellulose for
43
44 668 high-power supercapacitors. *Nano Res.* 10, 1847–1860.
45
46 669 <https://doi.org/10.1007/s12274-017-1573-8>
47
48 670 Liu, L., Ha, J., Hashida, T., Teramura, S., 2001. Development of a CO₂solidification
49
50 671 method for recycling autoclaved lightweight concrete waste. *J. Mater. Sci. Lett.* 20,
51
52 672 1791–1794. <https://doi.org/10.1023/A:1012591318077>
53
54 673 Ma, B., Ou, Z., Jian, S., Xu, R., 2011. Influence of cellulose ethers on hydration products
55
56
57
58
59
60
61
62
63
64
65

674 of portland cement. *J. Wuhan Univ. Technol. Mater. Sci. Ed.* 26, 588–593.
1
2 675 <https://doi.org/10.1007/s11595-011-0273-6>
3
4 676 Marsh, B.K., Day, R.L., 1988. Pozzolanic and cementitious reaction of fly ash in blended.
5
6 677 *Cem. Concr. Res.* 18, 301–310. <https://doi.org/https://doi.org/10.1016/0008->
7
8 678 [8846\(88\)90014-2](https://doi.org/10.1016/0008-8846(88)90014-2)
9
10 679 Mejdoub, R., Hammi, H., Suñol, J.J., Khitouni, M., Boufi, S., 2017. Nanofibrillated
11
12 cellulose as nanoreinforcement in Portland cement : Thermal , mechanical and
13 680
14 microstructural properties. *J. Compos. Mater.* 51, 2491–2503.
15 681
16 <https://doi.org/10.1177/0021998316672090>
17 682
18 683 Mikkelsen, D., Flanagan, B.M., Dykes, G.A., Gidley, M.J., 2009. Influence of different
19
20 carbon sources on bacterial cellulose production by *Gluconacetobacter xylinus* strain
21 684
22 ATCC 53524. *J. Appl. Microbiol.* 107, 576–583. <https://doi.org/10.1111/j.1365->
23 685
24 [2672.2009.04226.x](https://doi.org/10.1111/j.1365-2672.2009.04226.x)
25 686
26 687 Mohammadkazemi, F., Aguiar, R., Cordeiro, N., 2017. Improvement of bagasse fiber–
27
28 cement composites by addition of bacterial nanocellulose: an inverse gas
29 688
30 chromatography study. *Cellulose* 24, 1803–1814. <https://doi.org/10.1007/s10570->
31 689
32 [017-1210-4](https://doi.org/10.1007/s10570-017-1210-4)
33 690
34 691 Mohammadkazemi, F., Doosthoseini, K., Ganjian, E., Azin, M., 2015. Manufacturing of
35
36 bacterial nano-cellulose reinforced fiber-cement composites. *Constr. Build. Mater.*
37 692
38 101, 958–964. <https://doi.org/10.1016/j.conbuildmat.2015.10.093>
39 693
40 694 Moumin, M., Plank, J., 2017. Effectiveness of Polycarboxylate Dispersants in Enhancing
41
42 the Fluid Loss Performance of Cellulose Ethers. *SPE Int. Conf. Oilf. Chem.*
43 695
44 <https://doi.org/10.2118/184542-ms>
45 696
46 697 Muhd Julkapli, N., Bagheri, S., 2017. Nanocellulose as a green and sustainable emerging
47
48 material in energy applications: a review. *Polym. Adv. Technol.* 28, 1583–1594.
49 698
50 <https://doi.org/10.1002/pat.4074>
51 699
52 700 Nelson, E.B., 1990. *Well Cementing*. Elsevier.
53
54 701 Palou, M.T., Šoukal, F., Boháč, M., Šiler, P., Ifka, T., Živica, V., 2014. Performance of G-

- 702 Oil Well cement exposed to elevated hydrothermal curing conditions. *J. Therm. Anal.*
1
2 703 *Calorim.* 118, 865–874. <https://doi.org/10.1007/s10973-014-3917-x>
3
4 704 Pane, I., Hansen, W., 2005. Investigation of blended cement hydration by isothermal
5
6 705 calorimetry and thermal analysis. *Cem. Concr. Res.* 35, 1155–1164.
7
8 706 <https://doi.org/10.1016/j.cemconres.2004.10.027>
9
10 707 Parveen, S., Rana, S., Fangueiro, R., Conceiç, M., 2017. A novel approach of developing
11
12 708 micro crystalline cellulose reinforced cementitious composites with enhanced
13
14 709 microstructure and mechanical performance. *Cem. Concr. Compos.* 78.
15
16 710 <https://doi.org/10.1016/j.cemconcomp.2017.01.004>
17
18 711 Pourbeik, P., Alizadeh, R., Beaudoin, J.J., Nguyen, D.T., Raki, L., 2013. Microindentation
19
20 712 creep of 45 year old hydrated Portland cement paste. *Adv. Cem. Res.* 25, 301–306.
21
22 713 <https://doi.org/10.1680/adcr.12.00058>
23
24 714 Puertas, F., Santos, H., Palacios, M., Martínez-Ramírez, S., 2005. Polycarboxylate
25
26 715 superplasticiser admixtures: effect on hydration, microstructure and rheological
27
28 716 behaviour in cement pastes. *Adv. Cem. Res.* 17, 77–89.
29
30 717 <https://doi.org/10.1680/adcr.17.2.77.65044>
31
32 718 Ramasamy, J., Amanullah, M., 2020. Nanocellulose for oil and gas field drilling and
33
34 719 cementing applications. *J. Pet. Sci. Eng.* 184.
35
36 720 <https://doi.org/10.1016/j.petrol.2019.106292>
37
38 721 Saba, N., Tahir, P.M., 2016. A Review on Dynamic mechanical analysis of natural fibre
39
40 722 reinforced polymer composites. *Constr. Build. Mater.* 106, 149–159.
41
42 723 <https://doi.org/10.1016/j.conbuildmat.2015.12.075>
43
44 724 Salehi, S., Khattak, M., Ali, N., Rizvi, H., 2016. Laboratory Investigation of High
45
46 725 Performance Geopolymer Based Slurries AADE-16-FTCE-88. *Am. Assoc. Drill. Eng.*
47
48 726 Savastano, H., Warden, P.G., Coutts, R.S.P., 2005. Microstructure and mechanical
49
50 727 properties of waste fibre-cement composites, in: *Cement and Concrete Composites.*
51
52 728 pp. 583–592. <https://doi.org/10.1016/j.cemconcomp.2004.09.009>
53
54 729 Sereda, P.J., Feldman, R.F., Swenson, E.G., 1966. Effect of sorbed water on some
55
56
57
58
59
60
61
62
63
64
65

730 mechanical properties of hydrated Portland cement pastes and compacts. Highw.
 1
 2 731 Res. Board ... 58–73.
 3
 4 732 Sheykhnazari, S., Tabarsa, T., Ashori, A., Shakeri, A., Golalipour, M., 2011. Bacterial
 5
 6 733 synthesized cellulose nanofibers; Effects of growth times and culture mediums on
 7
 8 734 the structural characteristics. Carbohydr. Polym. 86, 1187–1191.
 9
 10 735 <https://doi.org/10.1016/j.carbpol.2011.06.011>
 11
 12 736 Sun, X., Wu, Q., Lee, S., Qing, Y., Wu, Y., 2016. Cellulose Nanofibers as a Modifier for
 13
 14 737 Rheology, Curing and Mechanical Performance of Oil Well Cement. Sci. Rep. 6, 1–
 15
 16 738 9. <https://doi.org/10.1038/srep31654>
 17
 18 739 Sun, X., Wu, Q., Zhang, J., Qing, Y., Wu, Y., Lee, S., 2017. Rheology, curing temperature
 19
 20 740 and mechanical performance of oil well cement: Combined effect of cellulose
 21
 22 741 nanofibers and graphene nano-platelets. Mater. Des. 114, 92–101.
 23
 24 742 <https://doi.org/10.1016/j.matdes.2016.10.050>
 25
 26 743 Tuutti, K., 1982. Corrosion of Steel in Concrete. Swedish Cem. Concr. Res. Inst. 469.
 27
 28 744 <https://doi.org/10.1002/9780470872864.ch49>
 29
 30 745 Vazquez, A., Foresti, M.L., Cerrutti, P., Galvagno, M., 2013. Bacterial Cellulose from
 31
 32 746 Simple and Low Cost Production Media by Gluconacetobacter xylinus. J. Polym.
 33
 34 747 Environ. 21, 545–554. <https://doi.org/10.1007/s10924-012-0541-3>
 35
 36 748 Vázquez, A., Pique, T.M., 2017. Biobased Additives in Oilwell Cement, in: Industrial
 37
 38 749 Applications of Renewable Biomass Products. Past, Present and Future. pp. 179–
 39
 40 750 198. <https://doi.org/10.1007/978-3-319-61288-1>
 41
 42 751 Wild, S., Khatib, J.M., 1997. Portlandite consumption in metakaolin cemen pastes and
 43
 44 752 mortars. Cem. Concr. Res. 27, 137–146.
 45
 46 753 [https://doi.org/https://doi.org/10.1016/S0008-8846\(96\)00187-1](https://doi.org/https://doi.org/10.1016/S0008-8846(96)00187-1)
 47
 48 754 Xiaofeng, C., Shanglong, G., Darwin, D., McCabe, S.L., 1990. Role of silica fume in
 49
 50 755 compressive strength of cement paste, mortar, and concrete. ACI Mater. J. 89, 375–
 51
 52 756 387. <https://doi.org/10.14359/2570>
 53
 54
 55
 56
 57
 58
 59

60 **757 Table captions**

1
2
3
4
5
6
7
8
9
10
11
12
13
14
15
16
17
18
19
20
21
22
23
24
25
26
27
28
29
30
31
32
33
34
35
36
37
38
39
40
41
42
43
44
45
46
47
48
49
50
51
52
53
54
55
56
57
58
59
60
61
62
63
64
65

758 Table 1. Cement chemical composition.

759 Table 2. Bacterial nanocellulose content in cement paste.

760 Table 3. Consistometry test.

761 Table 4. CH content and DOH (%) of the samples.

762 Table 5. BNC and SP percentages in cement samples.

763 **Figure captions**

764 Figure 1. Bacteria and bacterial nanocellulose (Courtesy of Cerruti et al. 2016)

765 Figure 2. Ultrasonic bath for homogenization of BNC - distilled water mixture.

766 Figure 3. Compressive strength test equipment.

767 Figure 4. Testing methodology.

768 Figure 5. Free fluid content for different percentages of superplasticizer for Portland
769 Cement (PC) and PC + 0.05% BNC.

770 Figure 6. Consistometry test for Portland Cement (PC), PC + 0.05% of BNC + 0.35% SP
771 and PC + 0.05% BNC + 0.40% SP.

772 Figure 7. (a) Example of mass loss calculation for CH in the TGA test (b)TGA results for
773 Portland Cement (PC) and PC modified with BNC at 0.05%, 0.10%, 0.15% and 0.20%
774 BWOC.

775
776 Figure 8. DrTGA results for Portland Cement (PC) and PC modified with BNC at 0.05%,
777 0.10%, 0.15% and 0.20% BWOC.

778 Figure 9. DMA results of Portland Cement (PC) and PC modified with BNC at 0.05%,
779 0.10%, 0.15% and 0.20% BWOC samples cured for 28 days.

780 Figure 10. Normalized storage modulus of Portland Cement (PC) and PC modified with
781 BNC at 0.05%, 0.10%, 0.15% and 0.20% BWOC samples cured for 28 days.

782 Figure 11 DMA results in term of tan δ of Portland Cement (PC) and PC modified with BNC
783 at 0.05%, 0.10%, 0.15% and 0.20% BWOC samples cured for 28 days.

784 Figure 12. Normalized compressive strength of Portland Cement (PC) and PC modified
 785 with BNC at 0.05%, 0.10%, 0.15% and 0.20% BWOC samples cured for 7 and 28 days as
 786 a function of the percentage of nanocellulose: Diamonds symbols represent samples cured
 787 for 7 days and squares symbols represent samples with 28 days of curing. The values have
 788 been normalized to the strength value obtained after 7 days of curing in PC cement.

789 Figure 13. Unconfined Compressive Strength for of Portland Cement (PC) and PC modified
 790 with BNC at 0.05%, 0.10%, 0.15% and 0.20% BWOC samples at three curing times: 8h, 7
 791 days and 28 days.

792 **Table 1.** Cement chemical composition.

Composition	CaO	SiO ₂	MgO	Al ₂ O ₃	Fe ₂ O ₃	SO ₃	Total alkali _{eq}
(wt%)	62.39	21.23	2.22	3.84	5.07	2.40	0.64

793 **Table 2.** Bacterial nanocellulose content in cement paste.

Mix	Additive [g]	BNC [g]	Added Water[g]	Water [g]	Total water [g]	Cement [g]	BNC content [%]
1	0	0	0	349	349	792	0.00
2	86.09	0.40	85.69	263.31	349	792	0.05
3	172.17	0.79	171.38	177.62	349	792	0.10
4	258.26	1.19	257.07	91.93	349	792	0.15
5	342.80	1.58	341.22	7.78	349	792	0.20

795 **Table 3.** Consistometry test.

Test	BNC [%]	SP [%]	Initial consistency [Bearden]	Thickening time [min]
1	0	0	15	99
2		0.05	Excessively viscous	-
3		0.15	Excessively viscous	-
4	0.05	0.3	Excessively viscous	-
5		0.35	35	99
6		0.4	12	126

796 **Table 4.** CH content and DOH (%) of the samples.

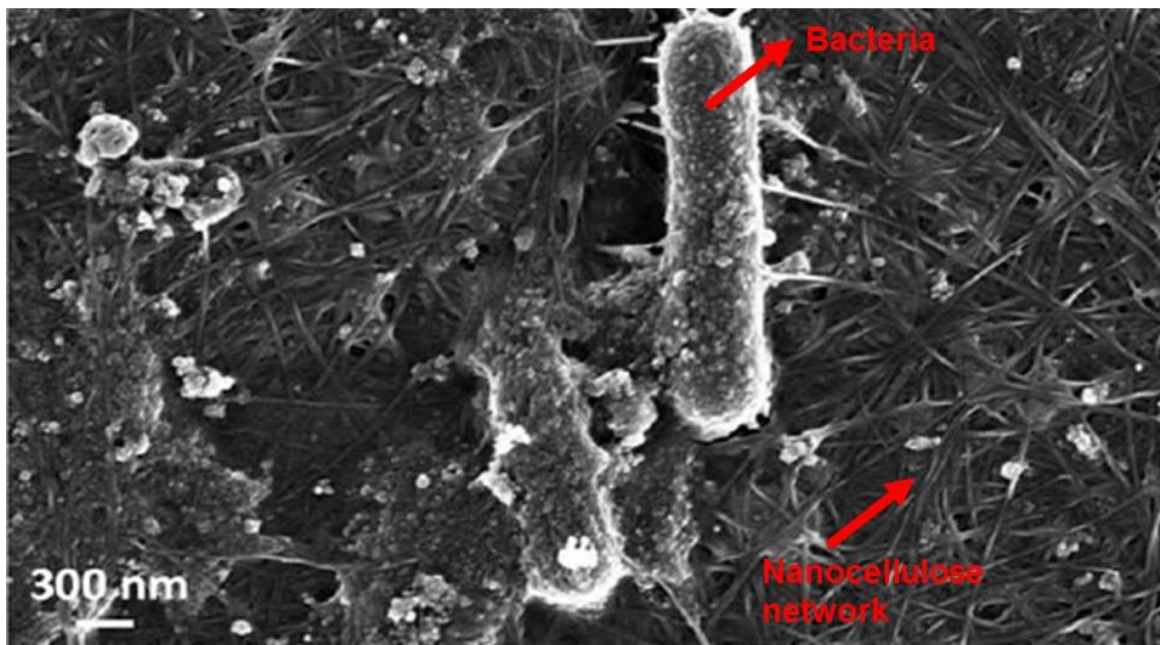
Sample	BNC [%]	CH [%]	DOH [%]
1	0	19.92%	62.96
2	0.05	22.16%	66.13
3	0.1	22.45%	64.62
4	0.15	22.67%	68.34
5	0.2	22.58%	66.88

797 **Table 5.** BNC and SP percentages in cement samples.

Sample	Cement [g]	Water [g]	Curing [days]	BNC [% BWOC]	SP [% BWOC]	
1	-	792	349	7	0	0
2	-	792	349	7	0.05	0.4
3	-	792	349	7	0.10	0.4

4	-	792	349	7	0.15	0.55
5	-	792	349	7	0.20	0.7
-	1	792	349	28	0	0
-	2	792	349	28	0.05	0.35
-	3	792	349	28	0.10	0.35
-	4	792	349	28	0.15	0.5
-	5	792	349	28	0.20	0.6

801
802



803
804
805

Figure 1. Bacteria and bacterial nanocellulose (Courtesy of Cerruti et al. 2016)



806

807

Figure 2. Ultrasonic bath for homogenization of BNC - distilled water mixture.

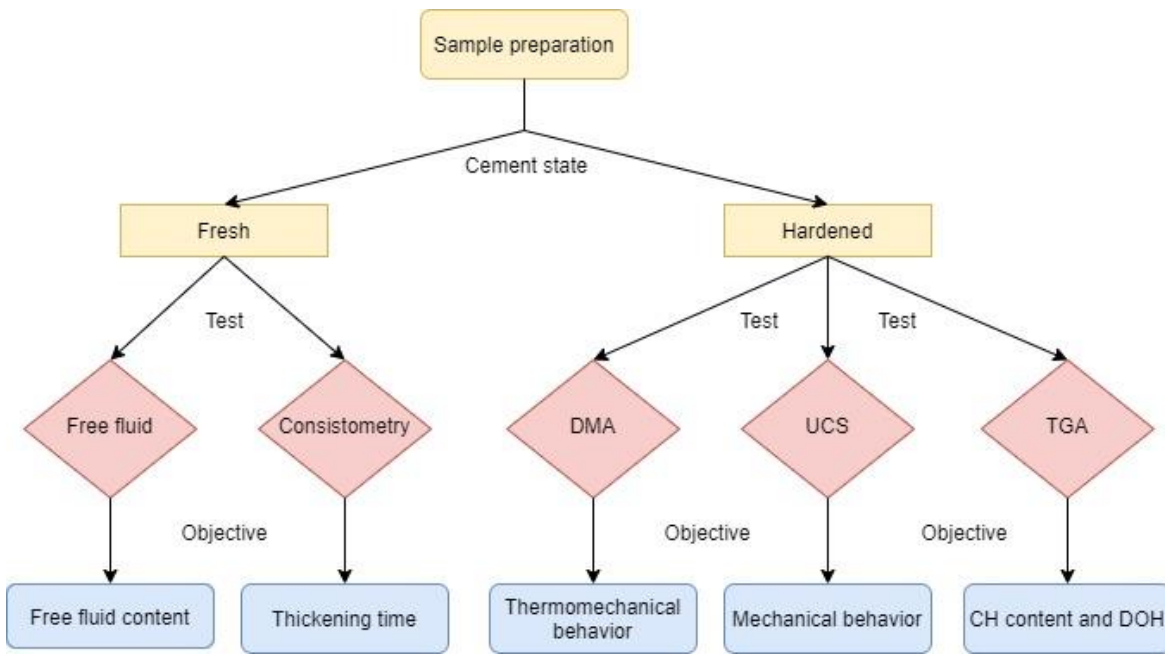


808

809

Figure 3. Compressive strength test equipment.

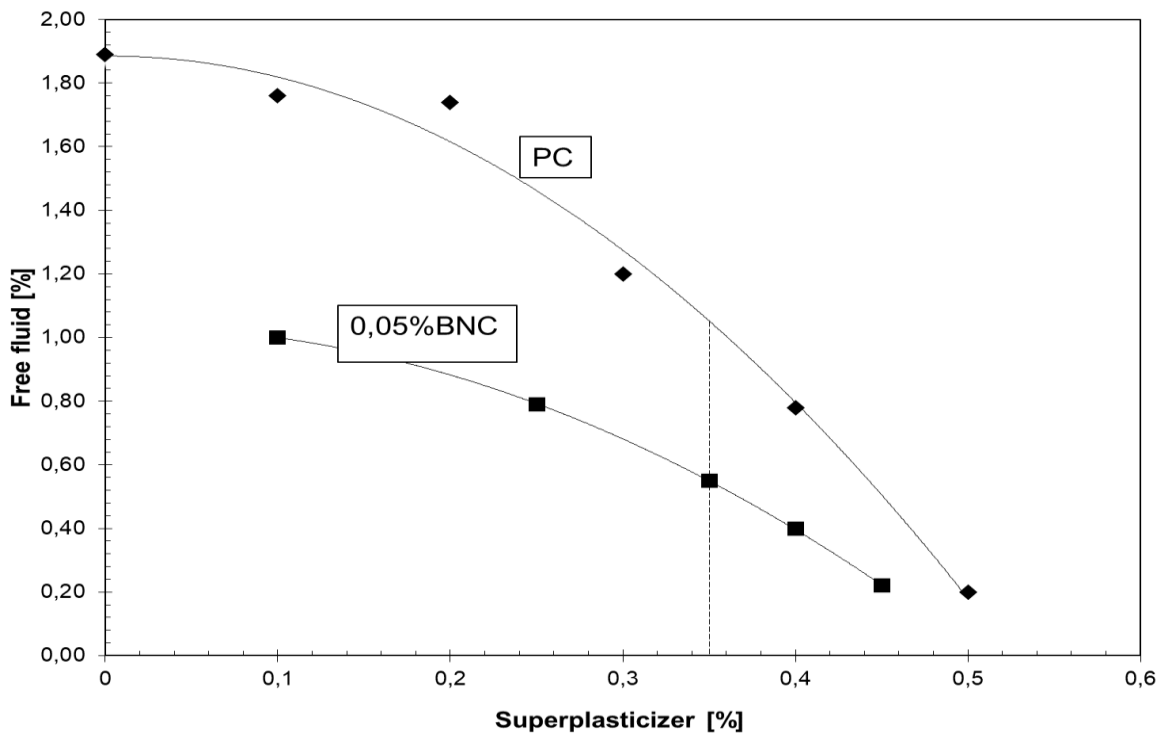
810



811

812 Figure 4. Testing methodology.

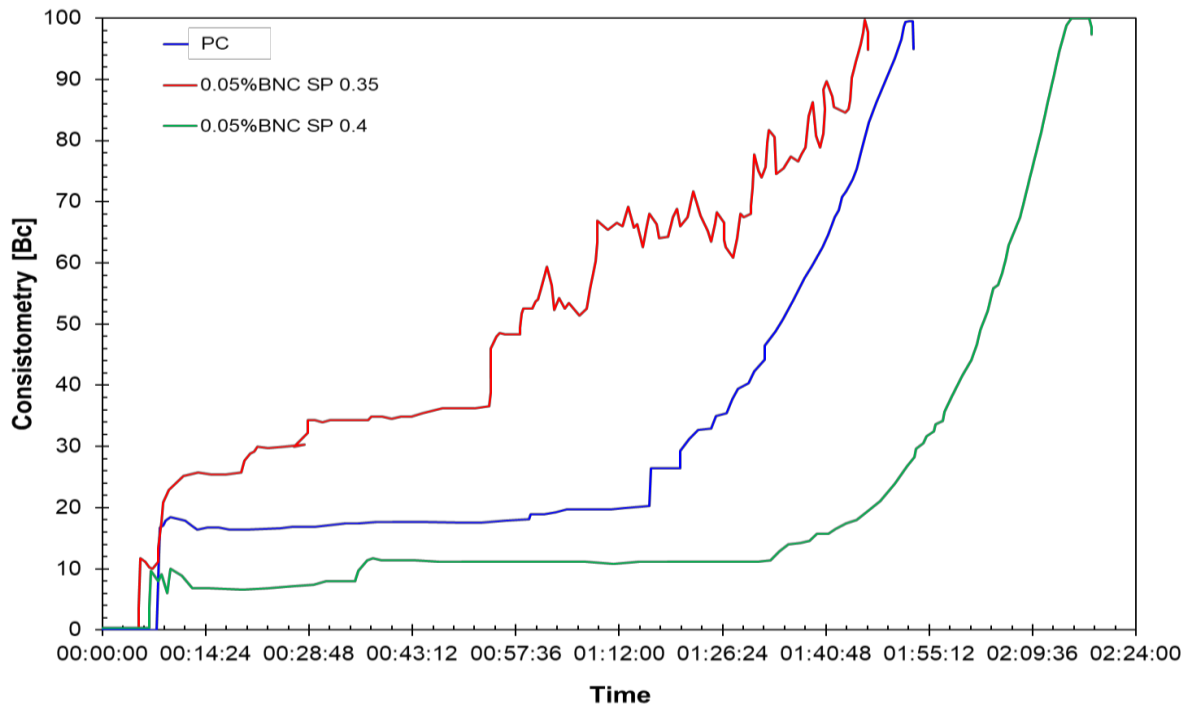
813



814

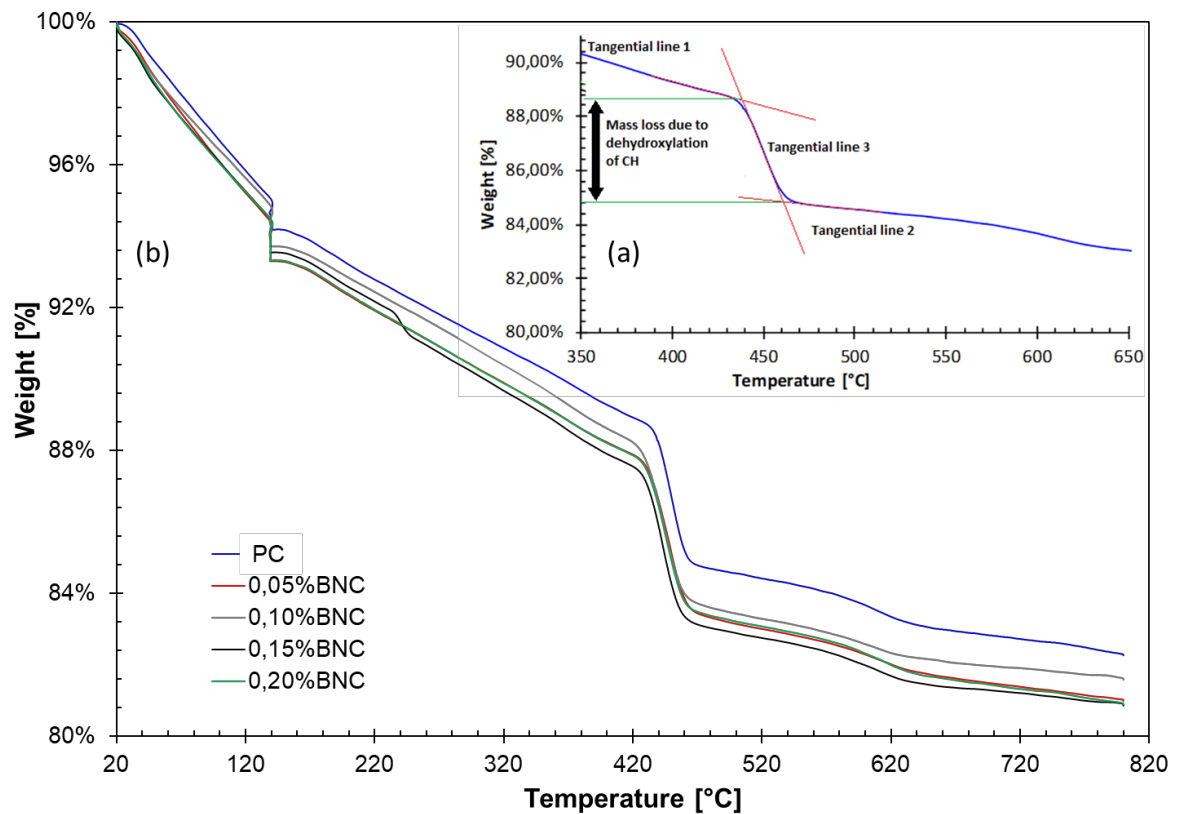
815 Figure 5. Free fluid content for different percentages of superplasticizer for Portland
816 Cement (PC) and PC + 0.05% BNC.

817



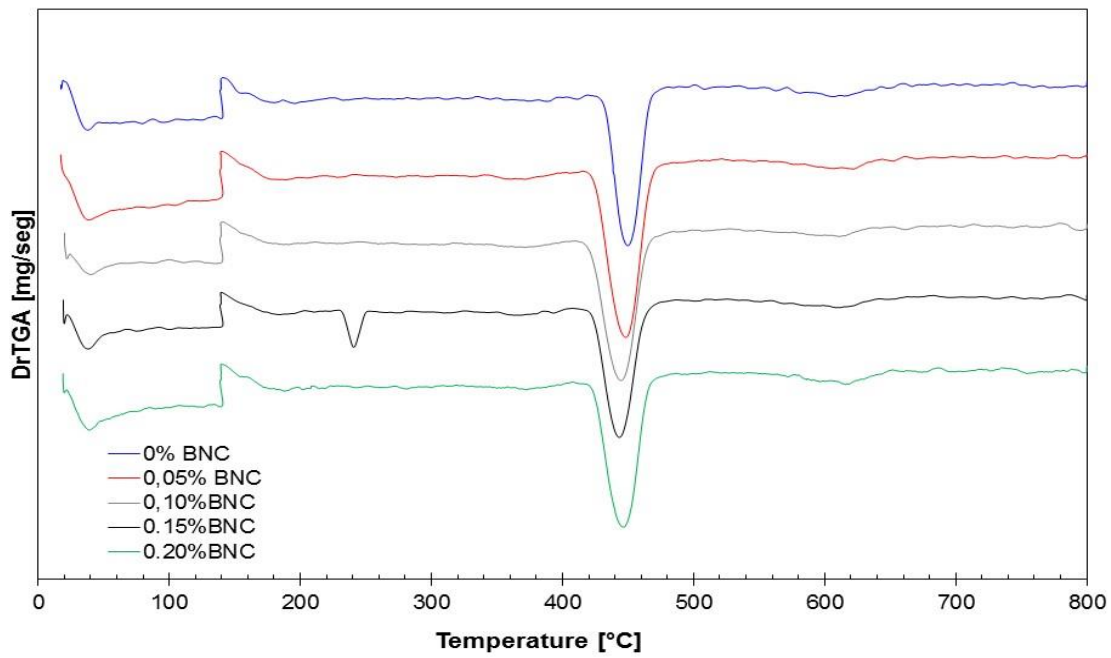
818

819 Figure 6. Consistometry test for Portland Cement (PC), PC + 0.05% of BNC + 0.35% SP
 820 and PC + 0.05% BNC + 0.40% SP.

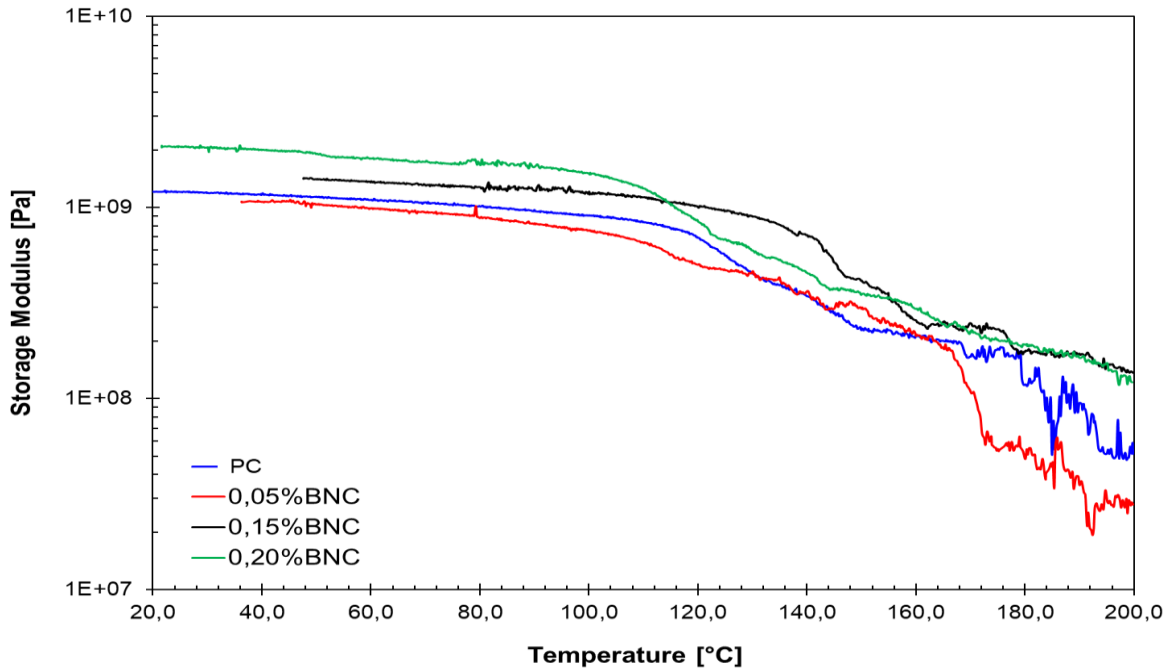


821

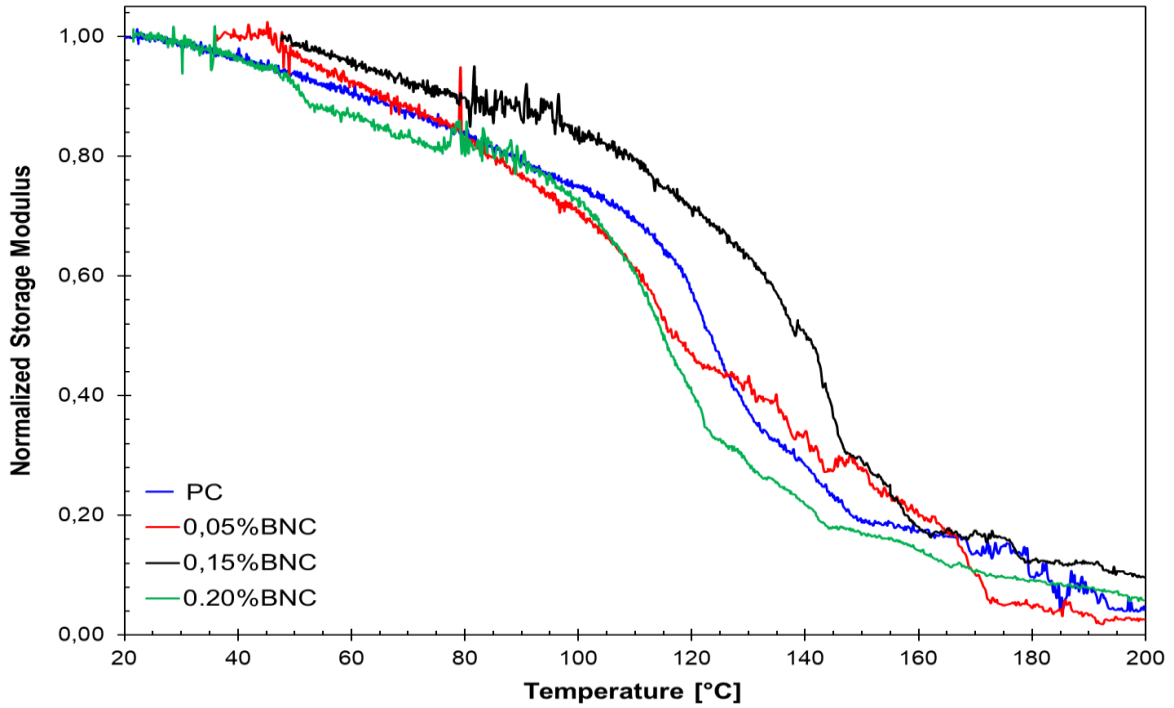
822 Figure 7. (a) Example of mass loss calculation for CH in the TGA test (b)TGA results for
 823 Portland Cement (PC) and PC modified with BNC at 0.05%, 0.10%, 0.15% and 0.20%
 824 BWOC.



825
 826 Figure 8. DrTGA results for Portland Cement (PC) and PC modified with BNC at 0.05%,
 827 0.10%, 0.15% and 0.20% BWOC.



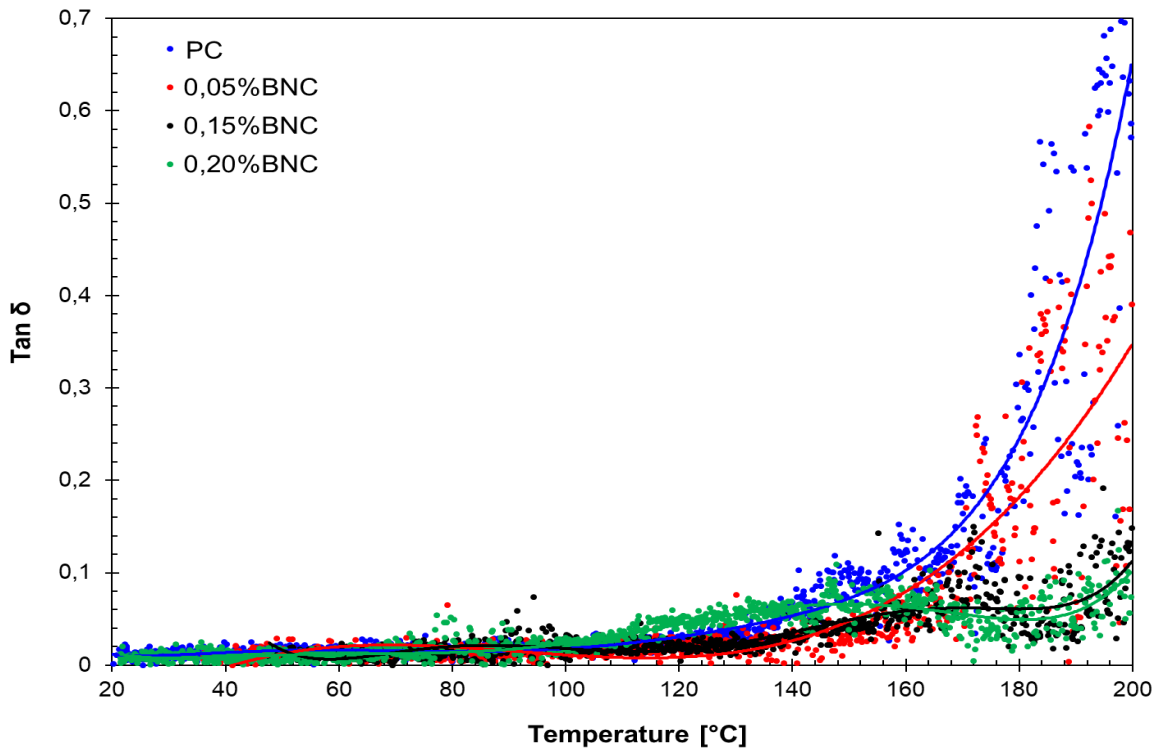
828
 829 Figure 9. DMA results of Portland Cement (PC) and PC modified with BNC at 0.05%,
 830 0.10%, 0.15% and 0.20% BWOC samples cured for 28 days.



831

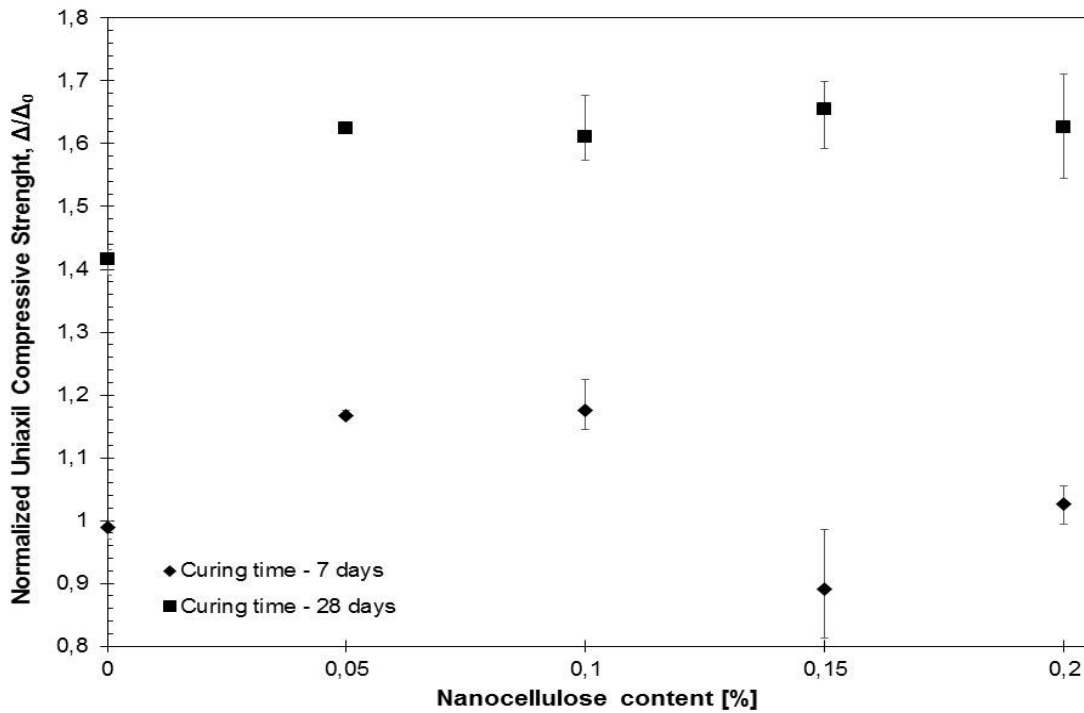
832 Figure 10. Normalized storage modulus of Portland Cement (PC) and PC modified with
 833 BNC at 0.05%, 0.10%, 0.15% and 0.20% BWOC samples cured for 28 days.

834



835

836 Figure 11. DMA results in term of $\tan \delta$ of Portland Cement (PC) and PC modified with BNC
 837 at 0.05%, 0.10%, 0.15% and 0.20% BWOC samples cured for 28 days.



838

839

840

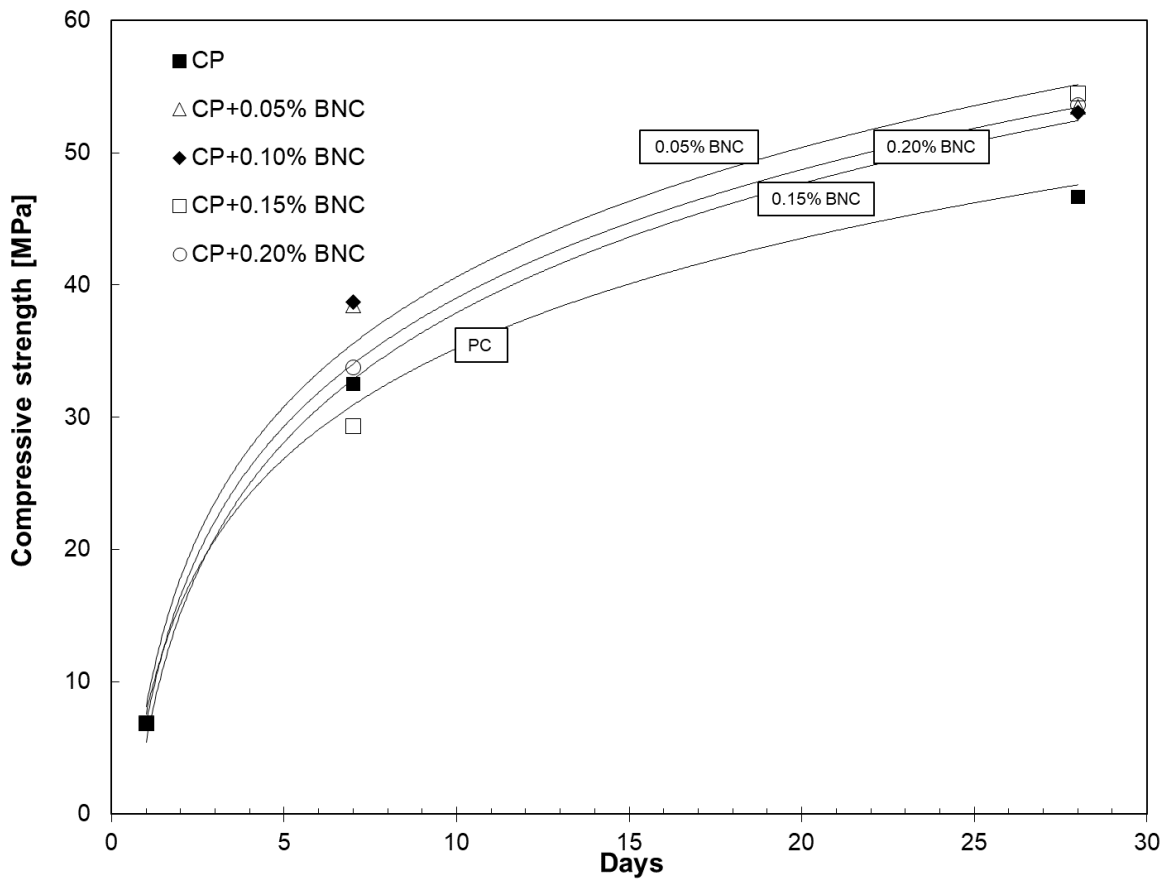
841

842

843

Figure 12. Normalized compressive strength of Portland Cement (PC) and PC modified with BNC at 0.05%, 0.10%, 0.15% and 0.20% BWOC samples cured for 7 and 28 days as a function of the percentage of nanocellulose: Diamonds symbols represent samples cured for 7 days and squares symbols represent samples with 28 days of curing. The values have been normalized to the strength value obtained after 7 days of curing in PC cement.

32
33
34
35
36
37
38
39
40
41
42
43
44
45
46
47
48
49
50
51
52
53
54
55
56
57
58
59
60
61
62
63
64
65



844

845

Figure 13. Unconfined Compressive Strength for of Portland Cement (PC) and PC modified with BNC at 0.05%, 0.10%, 0.15% and 0.20% BWOC samples at three curing times: 8h, 7 days, and 28 days. Only the average values of the results were considered.

847

848

Highlights

Incorporation of bacteria nano cellulose in oil-well cement improves the strength of hardened samples.

Thermogravimetric analysis shows an increment in hydration products and hydration degree with bacterial nanocellulose

Enhancement of thermal stability and tensile reinforcement has been observed using large percentages of bacterial nanocellulose.